Computational Mechanics 15 (1995) 473–484 © Springer-Verlag 1995

# A local coordinate system for assumed strain shell element formulation

**H. C. Park, S. W. Lee**



**Abstract** A new local coordinate system is introduced for the assumed strain formulation so that the resulting shell element can pass both the patch test and the locking test. The coordinate system is tested by implementing it in two nine-node assumed strain shell elements. The elements adopting the new local coordinate system not only pass various patch tests successfully but also perform well in locking tests.

## 1 Introduction

Various forms of assumed strain formulations have been widely used to construct plate and shell element models that are free of locking while kinematically stable. Lee and Pian (1978) introduced the assumed strain hybrid formulation based on the Hellinger-Reissner principle to construct finite element models for plates and shells. In this method, an independent strain field is assumed for each element in addition to an assumed displacement field. Subsequently, kinematically stable and locking free shell elements have been developed (Rhiu and Lee 1987; Yeom and Lee 1989; Yeom and Lee 1991; Chang et al. 1989; Bergmann and Mukherjee 1990). Other researchers (Jang and Pinsky 1987; Belytschko and Wong 1989; Huang and Hinton 1986; Park and Stanley 1986) used the displacement-dependent strain sampled at selected points for strain interpolation.

In the assumed strain formulation, a set of displacement-independent strains must be selected as simply as possible to alleviate locking. However, excessively simple assumed strain field may trigger spurious kinematic modes. These spurious modes must be suppressed because they may render a finite element model kinematically unstable. An assumed strain field to construct a locking free and kinematically stable element often becomes incomplete and non-symmetric in parent coordinates. Therefore, a local coordinate system must be defined such that the resulting element stiffness matrix can be invariant regardless of element node numbering. Different methods have been proposed to determine a local coordinate system which can result in a unique element stiffness matrix (Rhiu and Lee 1987; Yeom and Lee 1989; Yeom and Lee 1991). Previously, an analytical treatment of the kinematic stability and invariance of the finite element models based on the Hellinger-Reissner principle has been presented by Atluri and his associates (Rubenstein et al. 1982; Punch and Atluri 1984; Xue et al. 1985).

The assumed strain shell elements developed by Rhiu and Lee (1987) and Yeom and Lee (1989) are free of locking and kinematically stable. However, the local coordinate system proposed by Rhiu and Lee (1987) does not always result in a unique element stiffness matrix. In addition, the shell element produced cannot represent a constant stress or moment state for meshes of distorted elements. A local coordinate system which yields a unique element stiffness matrix was introduced by Yeom and Lee (1989); however, the element does not pass the patch tests. Subsequently, an alternate formulation was introduced by Yeom and Lee (1991), in which the independent strain field is assumed with respect to a local coordinate system defined at the centroid of the element. The resulting element passes the patch test successfully. However, this approach reintroduces locking.

In this paper, a new local coordinate system is introduced to obtain an invariant element that can pass both the patch and locking tests. The new local coordinate system is implemented in the two types of nine-node assumed strain shell elements (Yeom and Lee 1989; Park and Lee 1994). The effectiveness of the new approach is validated by conducting numerical tests on a set of example problems.

*Communicated by S. N. Atluri, 7 July 1994*

Department of Aerospace Engineering, University of Maryland, College Park, MD 20742, USA

The present work was supported in part by the Office of Naval Research (N0014-89-J-3059) with Dr. Roshdy Barsoum as the program monitor.

## 2
## Assumed strain formulation

An assumed strain finite element model can be constructed from the Hellinger-Reissner principle with an independent strain field as a variable in addition to a displacement field. Alternately, an equivalent element model can be constructed from the concept of strain substitution based on the principle of virtual work in combination with the least squares approximation for the assumed strain field. The equivalency of the two approaches can be demonstrated symbolically as follows.

For solids, the equilibrium equation is expressed in integral form as follows:

$$\int_V \delta \bar{\boldsymbol{\varepsilon}}^T \boldsymbol{\sigma} dV - \delta W = 0 \tag{1}$$



where $\delta \bar{\boldsymbol{\varepsilon}}$ is the virtual strain vector, $\boldsymbol{\sigma}$ is the stress vector, $\delta W$ is the virtual work due to applied load and $V$ is the volume. Introducing the displacement-independent strain $\boldsymbol{\varepsilon}$ in addition to the displacement-dependent strain $\bar{\boldsymbol{\varepsilon}}$ and the virtual stress $\delta \boldsymbol{\sigma}$, the compatibility condition in integral form is given as follows:

$$\int_V \delta \boldsymbol{\sigma}^T (\bar{\boldsymbol{\varepsilon}} - \boldsymbol{\varepsilon})\, dV = 0 \tag{2}$$

The stress-strain relationship for elastic materials is given as follows:

$$\boldsymbol{\sigma} = \mathbf{C}(\boldsymbol{\varepsilon} - \boldsymbol{\varepsilon}^{th}) \tag{3}$$

where C is the matrix of elastic constants and $\boldsymbol{\varepsilon}^{th}$ represents the thermally-induced strain. From Eq. (3), the virtual independent strain $\delta \boldsymbol{\varepsilon}$ is introduced as follows:

$$\delta \boldsymbol{\sigma} = \mathbf{C} \delta \boldsymbol{\varepsilon} \tag{4}$$

Substituting Eq. (3) in Eq. (1) and placing Eq. (4) into Eq. (2) lead to

$$\int_V \delta \bar{\boldsymbol{\varepsilon}}^T \mathbf{C} (\boldsymbol{\varepsilon} - \boldsymbol{\varepsilon}^{th})\, dV - \delta W = 0 \tag{5}$$

$$\int_V \delta \boldsymbol{\varepsilon}^T \mathbf{C} (\bar{\boldsymbol{\varepsilon}} - \boldsymbol{\varepsilon})\, dV = 0 \tag{6}$$

Within an element, the assumed displacement vector $\mathbf{u}$ can be symbolically expressed by the element nodal degrees of freedom $\mathbf{q}_e$ as follows:

$$\mathbf{u} = \mathbf{N} \mathbf{q}_e \tag{7}$$

where N is the shape function matrix. The displacement-dependent strain vector $\bar{\boldsymbol{\varepsilon}}$ can be written as

$$\bar{\boldsymbol{\varepsilon}} = \mathbf{B} \mathbf{q}_e \tag{8}$$

where B is a matrix of derivatives of the shape functions that relates the strain to the element nodal degrees of freedom. Similarly, the virtual displacement-dependent strain vector $\delta \bar{\boldsymbol{\varepsilon}}$ can be expressed as

$$\delta \bar{\boldsymbol{\varepsilon}} = \mathbf{B}\, \delta \mathbf{q}_e \tag{9}$$

where $\delta \mathbf{q}_e$ is the virtual element degrees of freedom.

In the formulation, an assumed strain field independent of the assumed displacment field is introduced for the construction of the element stiffness matrix. The independent strain vector $\boldsymbol{\varepsilon}$ is not required to be continuous across the element boundaries. Accordingly, it can be assumed within an element to be a combination of polynomial functions with unknown coefficients such that

$$\boldsymbol{\varepsilon} = \mathbf{P} \boldsymbol{\alpha} \tag{10}$$

where P is a matrix of assumed strain shape functions and $\boldsymbol{\alpha}$ is the vector of unknown coefficients. The virtual independent strain vector can then be expressed as follows:

$$\delta\boldsymbol{\varepsilon} = \mathbf{P}\,\delta\boldsymbol{\alpha} \tag{11}$$

Introducing Eqs. (8) and (10–11) into Eq. (6) leads to

$$\sum_i \delta\boldsymbol{\alpha}^T(\mathbf{G}\mathbf{q}_e - \mathbf{H}\boldsymbol{\alpha}) = 0 \tag{12}$$

where

$$\mathbf{G} = \int_{V_i} \mathbf{P}^T\mathbf{C}\mathbf{B}\,dV$$

$$\mathbf{H} = \int_{V_i} \mathbf{P}^T\mathbf{C}\mathbf{P}\,dV \tag{13}$$



Since $\delta\boldsymbol{\alpha}$ in Eq. (12) is an arbitrary quantity, $\boldsymbol{\alpha}$ is expressed as follows:

$$\boldsymbol{\alpha} = \mathbf{H}^{-1}\mathbf{G}\mathbf{q}_e \tag{14}$$

Substituting Eq. (14) into Eq. (10) leads to

$$\boldsymbol{\varepsilon} = \mathbf{P}\mathbf{H}^{-1}\mathbf{G}\mathbf{q}_e \tag{15}$$

Substituting Eqs. (9) and (15) into Eq. (5) leads to

$$\sum_i \delta\mathbf{q}_e^T(\mathbf{K}_e\mathbf{q}_e - \mathbf{Q}_{th} - \mathbf{Q}_{ex}) = 0 \tag{16}$$

where

$$\mathbf{K}_e = \mathbf{G}^T\mathbf{H}^{-1}\mathbf{G}$$

$$\mathbf{Q}_{th} = \int_V \mathbf{B}^T\mathbf{C}\boldsymbol{\varepsilon}^{th}\,dV \tag{17}$$

$$\delta\mathbf{q}_e^T\mathbf{Q}_{ex} = \delta W$$

In the above equation $\mathbf{K}_e$ is the element stiffness matrix, $\mathbf{Q}_{th}$ is the element nodal load vector due to the thermally-induced strain, and $\mathbf{Q}_{ex}$ is the element nodal load vector due to applied loads. The $\boldsymbol{\alpha}$ vector has been eliminated at the element level, and the resulting element stiffness matrix is defined with respect to the nodal degrees of freedom.

Alternately, the same finite element model can be obtained by replacing the displacement-dependent strain with a "substitute" strain based on the least squares approximation. With a substitute strain $\bar{\boldsymbol{\varepsilon}}$, a weighted least squares scalar function $L$ can be constructed as follows:

$$L = \int_V (\boldsymbol{\varepsilon} - \bar{\boldsymbol{\varepsilon}})^T\mathbf{C}(\boldsymbol{\varepsilon} - \bar{\boldsymbol{\varepsilon}})\,dV \tag{18}$$

The substitute strain can be assumed to be in a form as in equation (10). Introducing the assumed substitute strain and displacement-dependent strain, i.e. Eqs. (8) and (10) into Eq. (18) yields

$$L = \int_V (\mathbf{P}\boldsymbol{\alpha} - \mathbf{B}\mathbf{q}_e)^T\mathbf{C}(\mathbf{P}\boldsymbol{\alpha} - \mathbf{B}\mathbf{q}_e)\,dV \tag{19}$$

Minimizing Eq. (19) with respect to $\boldsymbol{\alpha}$ leads to

$$\boldsymbol{\alpha} = \mathbf{H}^{-1}\mathbf{G}\mathbf{q}_e \tag{20}$$

which is the same as Eq. (14). Substituting Eq. (20) into Eq. (10) yields

$$\boldsymbol{\varepsilon} = \mathbf{P}\mathbf{H}^{-1}\mathbf{G}\mathbf{q}_e \tag{21}$$

In terms of the substitute strain, the equilibrium Eq. (1) can be expressed as follows:

$$\int_V \delta\bar{\boldsymbol{\varepsilon}}^T \mathbf{C}(\boldsymbol{\varepsilon} - \boldsymbol{\varepsilon}^{th})\, dV - \delta W = 0 \tag{22}$$

which is identical to Eq. (5). Introducing Eqs. (9) and (21) into Eq. (22) and carrying out the integration yield



$$\sum_i \delta\mathbf{q}_e^T(\mathbf{K}_e\mathbf{q}_e - \mathbf{Q}_{th} - \mathbf{Q}_{ex}) = 0 \tag{23}$$

where

$$\mathbf{K}_e = \mathbf{G}^T\mathbf{H}^{-1}\mathbf{G} \tag{24}$$

The vectors $\mathbf{Q}_{th}$ and $\mathbf{Q}_{ex}$ are defined in Eq. (17). Note that the element stiffness matrix $\mathbf{K}_e$ is the same as that in Eq. (17).

Assembling all elements, Eq. (23) becomes

$$\delta\mathbf{q}^T(\mathbf{K}\mathbf{q} - \mathbf{Q}) = 0 \tag{25}$$

where $\mathbf{K}$ is the global stiffness matrix, $\mathbf{q}$ is the vector of the global nodal degrees of freedom, and $\mathbf{Q}$ is the global load vector. Since $\delta\mathbf{q}$ is an arbitrary quantity in Eq. (25),

$$\mathbf{K}\mathbf{q} = \mathbf{Q} \tag{26}$$

For the applied load, the vector $\mathbf{q}$ can be obtained by solving Eq. (26).

## 3
## Assumed strain for shell elements

For such locking sensitive cases as plate and shell formulations that include the effect of transverse shear deformation, the assumed strain field is chosen to avoid transverse shear or membrane locking while kinematic stability is maintained. To avoid locking, the assumed strain field must be chosen as simply as possible. However, spurious kinematic modes are triggered when an excessively simple form of the assumed strain field is assumed in the element. In this case, higher-order terms are added in the assumed strain field to suppress the spurious modes. Often this results in an assumed strain field which is incomplete and non-symmetric.

For example, consider a nine-node shell element with the mid-surface as shown in Fig. 1. the figure shows a shell mid-surface ($\zeta = 0$) with the global coordinates, $X$, $Y$, $Z$, local coordinate $x$, $y$, $z$, parent coordinates $\xi$, $\eta$, $\zeta$. Unit vectors $\mathbf{a}_1$ and $\mathbf{a}_2$ along $x$ and $y$, respectively, are tangential to the shell mid-surface while unit vector $\mathbf{a}_3$, along $z$, is normal to the surface.

In the degenerated solid shell concept, a line vector originally normal to the mid-surface is assumed to remain a line vector with no change in magnitude. Accordingly, the kinematics of deformation is

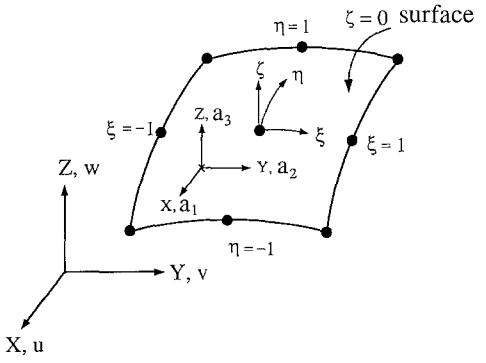


Fig. 1. The mid-surface of nine node shell element

described by five variables including three translational degrees of freedom and two angles representing the rotation of $\mathbf{a}_3$ vector. On the other hand, when the above assumption is abandoned, the rotation of $\mathbf{a}_3$ vector can be described by one vector. Three components of the vector are regarded as three degrees of freedom. This leads to an element with six degrees of freedom per node. (See Park and Lee 1994).

For the nine-node shell element with five degrees of freedom per node based on the degenerated solid concept, the following assumed strain field with 38 terms (38$\alpha$ version) has been found to be effective. (See Yeom and Lee 1991.)

$$
\begin{aligned}
\varepsilon_{xx} &= \alpha_1 + \alpha_2\xi + \alpha_3\eta + \alpha_4\xi\eta && + \alpha_{33}\underline{\xi\eta^2} \\
&\quad + \zeta(\alpha_5 + \alpha_6\xi + \alpha_7\eta + \alpha_8\xi\eta) && + \zeta\alpha_{37}\underline{\xi\eta^2} \\
\varepsilon_{yy} &= \alpha_9 + \alpha_{10}\xi + \alpha_{11}\eta + \alpha_{12}\xi\eta && + \alpha_{34}\underline{\xi^2\eta} \\
&\quad + \zeta(\alpha_{13} + \alpha_{14}\xi + \alpha_{15}\eta + \alpha_{16}\xi\eta) && + \zeta\alpha_{38}\underline{\xi^2\eta} \\
\varepsilon_{xy} &= \alpha_{17} + \alpha_{18}\xi + \alpha_{19}\eta + \alpha_{20}\xi\eta \\
&\quad + \zeta(\alpha_{21} + \alpha_{22}\xi + \alpha_{23}\eta + \alpha_{24}\xi\eta) \\
\varepsilon_{yz} &= \alpha_{25} + \alpha_{26}\xi + \alpha_{27}\eta + \alpha_{28}\xi\eta && + \alpha_{35}\underline{\xi^2\eta} \\
\varepsilon_{zx} &= \alpha_{29} + \alpha_{30}\xi + \alpha_{31}\eta + \alpha_{32}\xi\eta && + \alpha_{36}\underline{\xi\eta^2}
\end{aligned}
\tag{27}
$$

When the underlined terms are excluded, the assumed strain field in Eq. (27) is bilinear and symmetric in $\xi$ and $\eta$. However, the underlined terms are included to suppress the compatible kinematic modes without reintroducing element locking. Because of these underlined terms, the assumed strain field is incomplete and non-symetric. Consequently, the resulting element stiffness will not be invariant under the coordinate transformation unless special care is teken.

For the nine-node shell element with six degrees of freedom per node developed by Park and Lee (1994), the following assumed strain field with 52 terms (52$\alpha$ version) are used:

$$
\begin{aligned}
\varepsilon_{xx} &= \alpha_1 + \alpha_2\xi + \alpha_3\eta + \alpha_4\xi\eta && + \alpha_{45}\underline{\xi\eta^2} \\
&\quad + \zeta(\alpha_{25} + \alpha_{26}\xi + \alpha_{27}\eta + \alpha_{28}\xi\eta) && + \zeta\alpha_{49}\underline{\xi\eta^2} \\
\varepsilon_{yy} &= \alpha_5 + \alpha_6\xi + \alpha_7\eta + \alpha_8\xi\eta && + \alpha_{46}\underline{\xi^2\eta} \\
&\quad + \zeta(\alpha_{29} + \alpha_{30}\xi + \alpha_{31}\eta + \alpha_{32}\xi\eta) && + \zeta\alpha_{50}\underline{\xi^2\eta} \\
\varepsilon_{zz} &= \alpha_9 + \alpha_{10}\xi + \alpha_{11}\eta + \alpha_{12}\xi\eta \\
\varepsilon_{xy} &= \alpha_{13} + \alpha_{14}\xi + \alpha_{15}\eta + \alpha_{16}\xi\eta \\
&\quad + \zeta(\alpha_{33} + \alpha_{34}\xi + \alpha_{35}\eta + \alpha_{36}\xi\eta) \\
\varepsilon_{yz} &= \alpha_{17} + \alpha_{18}\xi + \alpha_{19}\eta + \alpha_{20}\xi\eta && + \alpha_{47}\underline{\xi^2\eta} \\
&\quad + \zeta(\alpha_{37} + \alpha_{38}\xi + \alpha_{39}\eta + \alpha_{40}\xi\eta) && + \zeta\alpha_{51}\underline{\xi^2\eta} \\
\varepsilon_{zx} &= \alpha_{21} + \alpha_{22}\xi + \alpha_{23}\eta + \alpha_{24}\xi\eta && + \alpha_{48}\underline{\xi\eta^2} \\
&\quad + \zeta(\alpha_{41} + \alpha_{42}\xi + \alpha_{43}\eta + \alpha_{44}\xi\eta) && + \zeta\alpha_{52}\underline{\xi\eta^2}
\end{aligned}
\tag{28}
$$

The above assumed strain field defined in the local coordinate system is incomplete and non-symmetric because of the underlined terms that are introduced to suppress the compatible kinematic modes. (See Park 1994 for detail.)

## 4
## Construction of a new local coordinate system

An assumed strain shell element which is invariant can be derived by using a local coordinate system carefully chosen at each integration point. To construct the local coordinate system, first a local coordinate

system is defined at the element centroid i.e. at the $\xi = \eta = \zeta = 0$ point. For this, the position vector of a point on the shell mid-surface $\mathbf{X}_0$ is expressed in terms of the nodal values as

$$\mathbf{X}_0 = \sum \mathbf{N}_i(\xi, \eta)\,(\mathbf{X}_0)_i \tag{29}$$

where $\mathbf{N}_i(\xi, \eta)$ is the mapping function corresponding to node $i$ and $(\mathbf{X}_0)_i$ is the value of $\mathbf{X}_0$ at node $i$. The unit vectors $\mathbf{v}_1$ and $\mathbf{v}_2$ are parallel to $\xi$ and $\eta$, respectively, and are defined at the centroid using the following equations.

$$\mathbf{v}_1 = \frac{\partial \mathbf{X}_0}{\partial \xi} \Big/ \left| \frac{\partial \mathbf{X}_0}{\partial \xi} \right|$$

$$\mathbf{v}_2 = \frac{\partial \mathbf{X}_0}{\partial \eta} \Big/ \left| \frac{\partial \mathbf{X}_0}{\partial \eta} \right| \tag{30}$$



Subsequently, the unit vector $\mathbf{v}_m$ is constructed by bisecting $\mathbf{v}_1$ and $\mathbf{v}_2$. The vector normal to the shell mid-surface $\mathbf{a}_3$ is obtained by taking cross product of $\mathbf{v}_1$ and $\mathbf{v}_2$ (Fig. 2). Now, $\mathbf{a}_1$ is constructed by bisecting $\mathbf{v}_m$ and $\mathbf{v}_m \times \mathbf{a}_3$. Finally, $\mathbf{a}_2$ is obtained by taking cross product of $\mathbf{a}_3$ and $\mathbf{a}_1$ as shown in Fig. 3.

Next, it is necessary to define a local coordinate system at other integration points. In this paper, the method previously used by Yeom and Lee (1989) is explained along with a new approach to define a local coordinate system at each integration point.

### 4.1
### Local coordinate system 1

A local orthogonal coordinate system at each integration point is defined following the same way used for the construction of a local coordinate system at the element centroid. As shown by Yeom and Lee (1989), the strain field in Eq. (27) is assumed with respect to the local orthogonal coordinate system defined in this fashion.

### 4.2
### Local coordinate system 2

In the new approach proposed in this paper, the $\mathbf{a}_3$ vector is first constructed at each integration point following the same way used to define $\mathbf{a}_3$ at the element centroid. The $\mathbf{a}_3$ vector at the element center ($\mathbf{a}_3^C$ in Figure 4) is then rotated to $\mathbf{a}_3$ at an integration point ($\mathbf{a}_3^G$). As $\mathbf{a}_3^C$ rotates to $\mathbf{a}_3^G$, $\mathbf{a}_1^C$ and $\mathbf{a}_2^C$ undergo rotations to generate $\mathbf{a}_1^G$ and $\mathbf{a}_2^G$ that are expressed by following equations described in Kane et al. (1987).

$$\mathbf{a}_1^G = \mathbf{a}_1^C \cos\theta - (\mathbf{a}_1^C \times \boldsymbol{\lambda}) \sin\theta + (\mathbf{a}_1^C \cdot \boldsymbol{\lambda})\,\boldsymbol{\lambda}(1 - \cos\theta)$$

$$\mathbf{a}_2^G = \mathbf{a}_2^C \cos\theta - (\mathbf{a}_2^C \times \boldsymbol{\lambda}) \sin\theta + (\mathbf{a}_2^C \cdot \boldsymbol{\lambda})\boldsymbol{\lambda}(1 - \cos\theta) \tag{31}$$

where

$$\boldsymbol{\lambda} = \mathbf{a}_3^C \times \mathbf{a}_3^G$$

$$\theta = \cos^{-1}(\mathbf{a}_3^C \cdot \mathbf{a}_3^G) \tag{32}$$

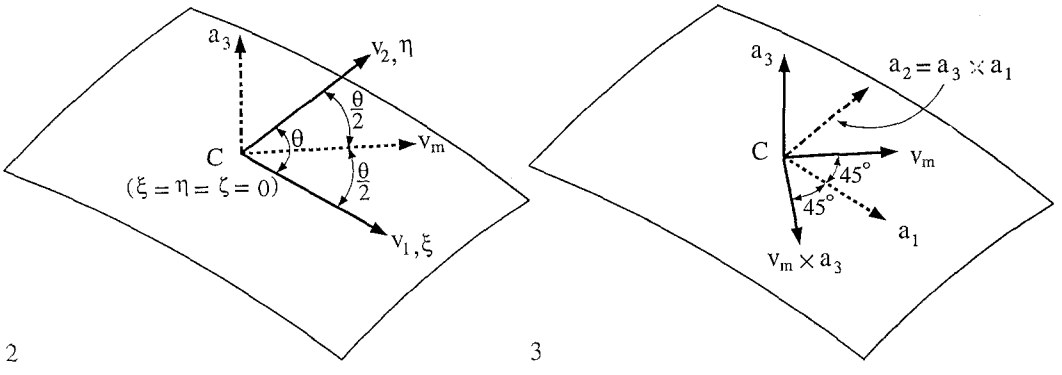


2 3

**Figs. 2, 3.** 2 Construction of $v_1$, $v_2$, $v_m$ and $a_3$ vectors at the element center. 3 Construction of a local coordinate system at the element center

In Eqs. (31–32) and Fig. 4, superscript 'G' indicates that the vector associated with it is defined at an integration point or Gauss point and superscript 'C' indicates the element center.

The two local coordinate systems become identical to each other when an element is flat and rectangular. When the element is used to model cylindrical shell structures using uniform meshes, the local coordinate system 1 turns out to be equal to the local coordinate system 2. However, the two local coordinate systems become distinct from each other when the element geometry is distorted.

## 5
## Numerical tests

Patch tests were performed to check the ability of the element models using local coordinate system 2 to represent constant stress or moment. In addition, locking tests were carried out to investigate whether the new local coordinate system 2 works well for thin plate and shell modeling. Depending on the local coordinate system implemented, the nine-node shell element with five degrees of freedom per node and the nine-node shell elements with six degrees of freedom per node are designated as follows:



| Element designation | Local coordinate system | DOF per node |
|---|---|---|
| C1/5 | 1 | 5 |
| C2/5 | 2 | 5 |
| C2/6 | 2 | 6 |

In the tables that follow, the result for 'C1/5' is taken from Yeom and Lee (1991) where it is presented as 'OLD'. The material properties used in the numerical tests except for the beam with 90° pre-twist are Young's modulus $E = 10 \times 10^6$ and Poisson's ratio $\nu = 0.3$

## 6
## Patch tests

*A reactangular plate under uniform tension* A rectangular plate is under uniform tension $p_x = 1$ (psi) as shown in Fig. 5. Using the symmetry in geometry and loading, a quarter of the plate is modeled by

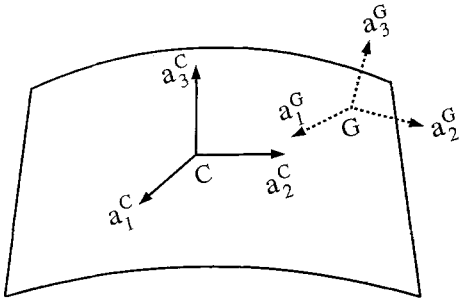


Fig. 4. Construction of a local coordinate system at an integration point

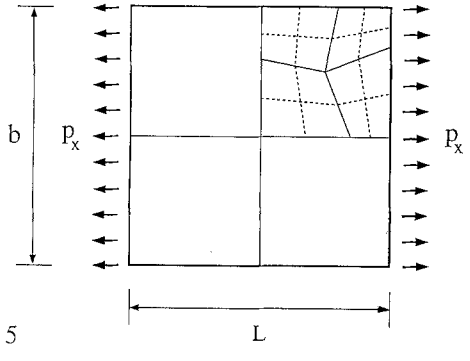


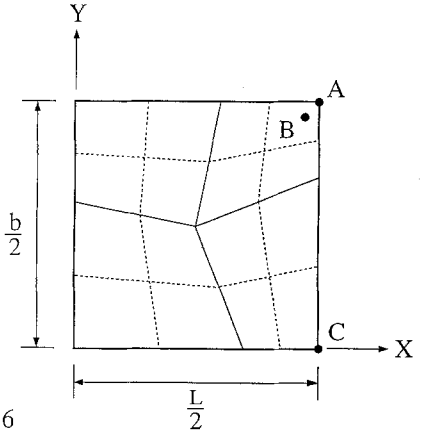


Figs. 5, 6. A rectangular plate under uniform tension. 6 D2 × 2 and D4 × 4 meshes

distorted 2 × 2 and 4 × 4 meshes that are denoted by D2 × 2 and D4 × 4, respectively, as shown in Fig. 6. The dimensions of the plate are $L = b = 2$ (in) and the plate thickness is $t = 0.02$ (in) resulting in a $L/b$ ratio of 1 and a $b/t$ ratio of 100.

The horizontal displacement at the plate corner $A$ is normalized by the exact solution $U_{exact} = p_x L / (2E)$. The normalized horizontal displacement at the plate corner $A$ is denoted by $U_A$ in Table 1. Axial stress evaluated at the integration point $B$ is also normalized by the exact solution and denoted by $(\sigma_{xx})_B$. As shown in Table 1, the C2/5 and C2/6 elements represent the constant stress state even for the distorted meshes. On the other hand, the C1/5 element adopting the local coordinate system 1 fails to represent the constant stress state when this example is modeled by distorted meshes.



***A rectangular plate under uniform bending*** A uniform bending moment per unit length $M_x = 1$ (lb-in/in) is applied along the edges of a rectangular plate (Fig. 7). As in the previous example, a quarter of the plate is modeled by distorted 2 × 2 and 4 × 4 meshes (D2 × 2, D4 × 4 in Fig. 6) to check whether the element can represent a constant moment state.

The length in the Y direction is fixed as $b = 2$ (in) and the length in the X direction, $a$, is given such that the resulting aspect ratio $a/b = 1, 2$. The plate thickness is given as $t = 0.02$ (in) resulting in the $b/t$ ratio of 100.

The lateral displacement at the plate corner C is normalized by exact solution (Timoshenko and Woinowsky 1959). The moments $M_x$ and $M_y$ at the integration point B are normalized by applied $M_x$. Figure 6 shows the location of points B and C. The normalized lateral displacement is denoted by $W_C$ and the normalized moments are denoted by $(M_x)_B$ and $(M_y)_B$ in Table 2. Note that, in contrast to the C1/5 model using the local coordinate system 1, the C2/5 and C2/6 element models represent constant moment state even when distorted meshes are used.

Table 1. Normalized horizontal displacement and stress

| Mesh | Element model | $U_A$ | $(\sigma_{XX})_B$ |
|---|---|---|---|
| D2 × 2 | C1/5 | 0.9968 | 0.9974 |
| | C2/5 | 1.0000 | 1.0000 |
| | C2/6 | 1.0000 | 1.0000 |
| D4 × 4 | C1/5 | 0.9995 | 0.9994 |
| | C2/5 | 1.0000 | 1.0000 |
| | C2/6 | 1.0000 | 1.0000 |

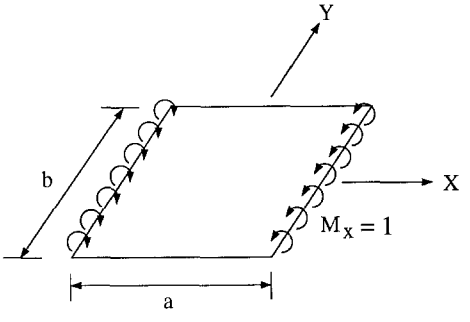


Fig. 7. A plate under bending moment

Table 2. Normalized lateral displacement and moment resultant for $M_x = 1$

| $a/b$ | Element model | D2 × 2 | | | D4 × 4 | | |
|---|---|---|---|---|---|---|---|
| | | $W_C$ | $(M_x)_B$ | $(M_y)_B$ | $W_C$ | $(M_x)_B$ | $(M_y)_B$ |
| 1 | C1/5 | 1.0005 | 0.9992 | 0.0011 | 1.0001 | 0.9995 | −0.0003 |
| | C2/5 | 1.0000 | 1.0000 | 0.0000 | 1.0000 | 1.0000 | 0.0000 |
| | C2/6 | 1.0000 | 1.0000 | 0.0000 | 1.0000 | 1.0000 | 0.0000 |
| 2 | C1/5 | 1.0005 | 0.9858 | −0.0025 | 1.0000 | 0.9954 | −0.0009 |
| | C2/5 | 1.0000 | 1.0000 | 0.0000 | 1.0000 | 1.0000 | 0.0000 |
| | C2/6 | 1.0000 | 1.0000 | 0.0000 | 1.0000 | 1.0000 | 0.0000 |

*A circular ring under uniform internal pressure* A circular ring of radius $R = 100$ (in), width $b = 1$ (in) and thickness $t = 1$ (in) is under uniform internal pressure (Fig. 8). Due to the symmetry in geometry and loading, a 5° section of the ring with width of $b/2$ is divided by two uniform elements (U2) and two distorted elements (D2). The D2 mesh is made such that the angle between line BE and AC is 60° when the 5° section is stretched on a flat plane (Fig. 9).

The radial displacement at the corner $A$ and hoop stress at the integration point $F$ are normalized by the corresponding exact solutions in Boresi et al. (1978). The normalized radial displacement and hoop stress are denoted by $W_A$ and $(\sigma_{\theta\theta})_F$, respectively in Table 3. Note that the C1/5 model can not represent constant stress state when distorted meshes are used. The element models using the local coordinate system 2 have the ability to represent the constant stress state.

*A sphere under uniform external pressure* As shown in Fig. 10, a sphere of radius $R = 10$ (in) and thickness $t = 0.1$ (in) ($R/t = 100$) is under uniform external pressure $p_r = 1$ (psi). Using the symmetry in geometry and loading, a $\phi = \theta = 2°$ portion is modeled for this example. The section is divided by a $2 \times 2$ uniform mesh (U2 × 2) and a $2 \times 2$ distorted mesh (D2 × 2). The $2 \times 2$ distorted mesh is constructed such that the angle $\gamma = 60°$ when it is stretched on a flat plane (Fig. 11).

Table 4 lists the radial displacement ($U_r$) at the node point $A$ and tangential stresses ($\sigma_{\phi\phi}$ and $\sigma_{\theta\theta}$) at the integration point $G$ normalized by the corresponding exact solutions provided in Roark and Young (1975). The radial displacement at every nodal point is identical due to the symmetry in geometry and



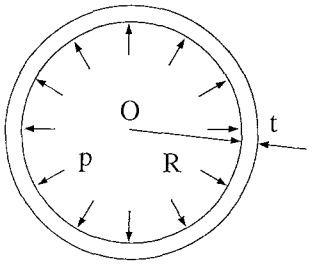


8

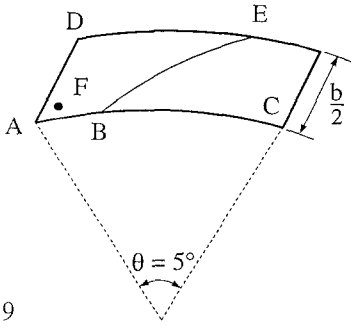


9

**Figs. 8, 9.** 8 A ring under uniform internal pressure. 9 A D2 mesh for 5° section of the ring

| Mesh | Element model | $W_A$ | $(\sigma_{\theta\theta})_F$ |
|---|---|---|---|
| U2 | C1/5 | 1.0000 | 1.0000 |
| | C2/5 | 1.0000 | 1.0000 |
| | C2/6 | 1.0000 | 1.0000 |
| D2 | C1/5 | 1.0022 | 1.0120 |
| | C2/5 | 1.0000 | 1.0000 |
| | C2/6 | 1.0000 | 1.0000 |

**Table 3.** Normalized radial displacement and hoop stress

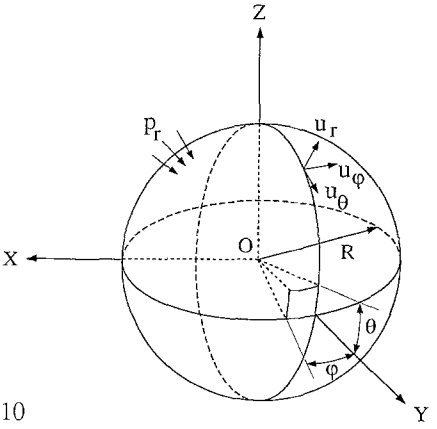


10

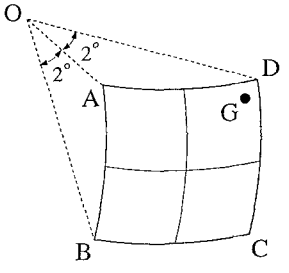


11a

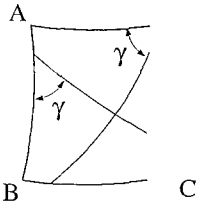


b

**Figs. 10, 11.** 10 A sphere under uniform external pressure. 11 a A uniformly divided $2 \times 2$ mesh b A distorted $2 \times 2$ mesh

loading. Tangential stresses at every integration point inside any element are also equal to each other. The results shown are obtained using the nine-node element with six degrees of freedom per node in which the local coordinate system 2 is adopted (C2/6). This example shows that the element model C2/6 has the ability to represent constant stress state.

## 7 Locking test

*A clamped square plate under uniform pressure* A square plate clamped along the four edges is under uniform pressure (Fig. 12). Using the symmetry, a quarter of the plate is modeled by distorted D2 × 2 and D4 × 4 meshes as well as uniform U2 × 2 and U4 × 4 meshes. The D2 × 2 and D4 × 4 meshes are the same as those used in the previous examples (Fig. 6). The side lengths of the plate are $a = b = 2$ (in) and the plate thickness $t$ is given as 0.02, 0.002 and 0.0002 (in).



The maximum displacement at the plate center is normalized by the exact solution (Timoshenko and Woinowsky 1959) and listed in Table 5. When uniform meshes are used, all three element models give the same results. However, the result obtained by C2/6 is slightly better than those obtained by C1/5 and C2/5, when D4 × 4 mesh is used for $b/t = 10^3$ and $10^4$ cases.

*A pinched circular ring* A circular ring is subjected to a pair of concentrated loads $P = 1$ (lb) as shown in Fig. 13. The dimensions of the ring are radius $R = 100$ (in), width $b = 1$ (in) and thicknesses are given as $t = 1, 0.2, 0.1$ (in). Using the symmetry of geometry and loading, only one eighth of the ring is modeled with meshes of distorted elements (D4 and D8) as well as a mesh of four uniformly divided elements (U4).

The U4 mesh is constructed by dividing one eighth of the ring into four uniform elements in the circumferential direction. Figure 14 shows the D4 and D8 meshes for the section. For the D4 mesh, the

Table 4. Normalized radial displacement $U_r$ and tangential stresses $\sigma_{\phi\phi}$, $\sigma_{\theta\theta}$

| | U2 × 2 | D2 × 2 |
|---|---|---|
| $U_r$ | 1.000 | 1.000 |
| $\sigma_{\phi\phi}$ | 1.000 | 1.000 |
| $\sigma_{\theta\theta}$ | 1.000 | 1.000 |

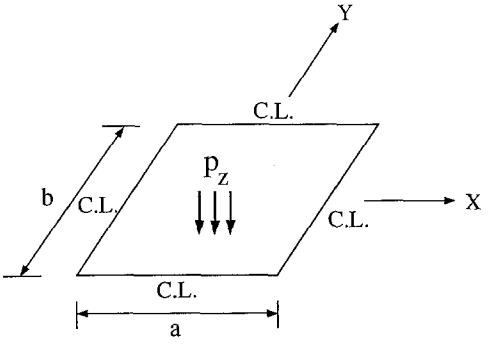


Fig. 12. A clamped square plate under uniform pressure

Table 5. Normalized lateral displacement at the square plate center

| $b/t$ | Element model | U2 × 2 | U4 × 4 | D2 × 2 | D4 × 4 |
|---|---|---|---|---|---|
| $10^2$ | C1/5 | 1.0131 | 1.0029 | 0.9955 | 1.0011 |
| | C2/5 | 1.0131 | 1.0029 | 0.9962 | 1.0004 |
| | C2/6 | 1.0131 | 1.0029 | 1.0186 | 1.0035 |
| $10^3$ | C1/5 | 1.0111 | 1.0009 | 0.8421 | 0.9857 |
| | C2/5 | 1.0111 | 1.0009 | 0.8517 | 0.9858 |
| | C2/6 | 1.0111 | 1.0009 | 0.9239 | 0.9976 |
| $10^4$ | C1/5 | 1.0111 | 1.0009 | 0.5801 | 0.9345 |
| | C2/5 | 1.0111 | 1.0009 | 0.2324 | 0.9435 |
| | C2/6 | 1.0111 | 1.0009 | 0.2282 | 0.9854 |

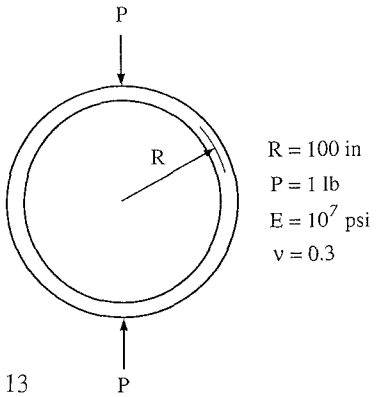


13

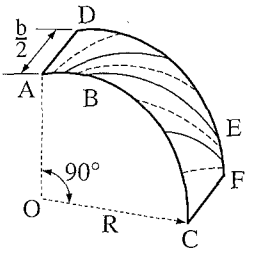


14

Figs. 13, 14. 13 A pinched ring. 14 The D4 and D8 meshes for 1/8 of the ring

Table 6. Normalized displacement at the loading point

| *R/t* | Element model | U4 | D4 | D8 |
|---|---|---|---|---|
| 100 | C1/5 | 1.0008 | 1.0007 | 1.0002 |
| | C2/5 | 1.0008 | 0.9991 | 1.0000 |
| | C2/6 | 0.9983 | 0.9970 | 0.9996 |
| 500 | C1/5 | 1.0006 | 0.9953 | 0.9993 |
| | C2/5 | 1.0006 | 0.9828 | 0.9970 |
| | C2/6 | 0.9981 | 0.9861 | 0.9973 |
| 1000 | C1/5 | 1.0004 | 0.9857 | 0.9977 |
| | C2/5 | 1.0004 | 0.9530 | 0.9917 |
| | C2/6 | 0.9981 | 0.9711 | 0.9933 |

angle EBC is 60° when the modeled section of the ring is stretched on a flat plane. The D8 mesh is constructed by dividing the D4 mesh along the dotted lines.

The radial displacement at the loading point is normalized by the exact solution (Lee and Pian 1978) and listed in Table 6. For the distorted mesh, the C1/5 model appears to work slightly better than the C2/5 and C2/6 models. However, the differences are negligible.

***A 90° pre-twisted cantilever beam under tip loads*** A 90° pre-twisted cantilever beam is under forces applied at the beam tip in the Y or Z direction as shown in Fig. 15. Tip displacements in the corresponding loading directions for two loading cases (a) and (b) are calculated for two beams with different thicknesses.

Table 7 lists the tip displacements in the Y and Z directions for the loads in the Y and Z directions, respectively. The displacements are obtained using the nine-node shell element with six degrees of freedom per node (C2/6) and normalized with respect to exact solutions provided in Belyschko and Wong (1989). The numerical solutions agree very well with exact solutions even for a very thin beam.

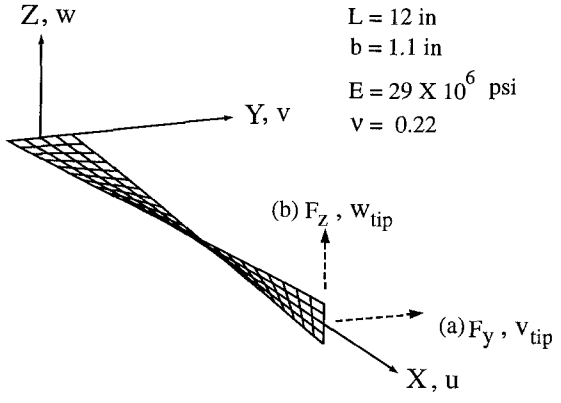


Fig. 15. A 90° pre-twisted cantilever beam under tip forces

Table 7. Normalized tip displacement of a 90° pre-twisted cantilever beam

| Mesh size | $t = 0.32$ in | | $t = 0.0032$ in | |
|---|---|---|---|---|
| | (a) $V_{tip}$ | (b) $W_{tip}$ | (a) $V_{tip}$ | (b) $W_{tip}$ |
| $6 \times 1$ | 1.00472 | 1.00753 | 1.00320 | 0.99683 |
| $12 \times 1$ | 1.00140 | 1.00131 | 1.00984 | 1.00355 |
| $12 \times 2$ | 1.00066 | 1.00103 | 1.00420 | 1.00255 |



## 8 Conclusion

In the present paper, a new method to determine a local coordinate system is proposed and examined by implementing it in two nine-node assumed strain shell elements. From the patch tests, the shell elements C2/5 and C2/6 employing the new local coordinate system demonstrate their ability to represent constant stress or moment state. In addition, the C2/5 and C2/6 models are insensitive to shear and membrane locking. This indicates that the new local coordinate system removes the shortcomings of the local coordinate system used in the C1/5 model without reintroducing element locking.

## References

**Bergmann, V. L.; Mukherjee, S.** 1990: A hybrid strain finite element for plates and shells. Int. J. Num. Meth. Eng. 30: 233–257

**Boresi, A. P.; Sidebottom, O. M.; Seely, F. B.; Smith, J. O.** 1978: Advanced mechanics of materials, 3rd. Ed. New York: John Wiley and Sons

**Belytschko, T.; Wong, B. L.** 1989: Assumed strain stabilization procedure for the 9-Node lagrange shell element. Int. J. Num. Meth. Eng. 28: 385–414

**Chang, T. Y.; Saleeb, A. F.; Graf, W.** 1989: On the mixed formulation of a 9-Node lagrange shell element. Comp Meth. Appl. Mech. Eng. 73: 259–281

**Huang, H. C.; Hinton, E. H.** 1986: A new nine node degenerated shell element with enhanced membrane and shear interpolation. Int. J. Num. Meth. Eng. 22: 73–92

**Jang, J.; Pinsky, P. M.** 1987: An assumed covariant strain based 9-Node shell element. Int. J. Num. Meth. Eng. 24: 2389–2411

**Kane, T. R.; Linkins, P. W.; Levinson, D. A.** 1983: Spacecraft dynamics, New York: McGraw-Hill

**Lee, S. W.; Pian, T. H. H.** 1978: Improvement of plate and shell finite element by mixed formulations. AIAA J., 16: 29–34

**Park, K. C.; Stanley, G. M.** 1986: A curved $C^0$ shell element based on assumed natural-coordinate strains. J. Appl. Mech. 53: 278–290

**Park, H. C.; Lee, S. W.** 1994: Geometrically nonlinear assumed strain shell element model with six degrees of freedom per node. 35th AIAA/ASME/ASCE/AHS structures, structural dynamics and materials conference, Hilton Head, SC, U.S.A., April 18–21

**Park, H. C.** 1994: An efficient geometrically nonlinear assumed strain shell element model with six degrees of freedom per node. Ph.D. Dissertation, Dept. Aero., Univ., of Maryland

**Punch, E. F.; Atluri, S. N.** 1984: Development and testing of stable, invariant, isoparametric curvilinear 2- and 3-D hybrid-stress elements. Comp. Meth. Appl. Mech. Eng. 47: 331–356

**Rhiu, J. J.; Lee, S. W.** 1987: A new efficient mixed formulation for thin shell finite element models. Int. J. Num. Meth. Eng. 24: 581–604

**Roark, R. J.; Young, W. C.** 1975: Formulars for stress and strain, 5th. Ed.: McGraw-Hill

**Rubenstein, R.; Punch, E. F.; Alturi, S. N.** 1982: An analysis of, and remedies for, kinematic modes in hybrid-stress finite elements: selection of stable, invariant stress fields. Comp. Meth. Appl. Mech. Eng. 38: 63–92

**Timoshenko, S. P.; Woinowsky-Krieger, S.** 1959: Theory of plate and shells, 2nd Ed., New York: McGraw-Hill

**Xue, W. M.; Karlovitz, L. A.; Atluri, S. N.** 1985: On the Existence and Stability Conditions for Mixed-Hybrid Finite Element Solutions based on Reissner's Variational Principle. *Int. J. Solids and Structures*, 21: 97–116

**Yeom, C. H.; Lee, S. W.** 1989: An assumed strain element model for large deflection composite shells. Int. J. Num. Meth. Eng. 28: 1749–1768

**Yeom, C. H.; Lee, S. W.** (1991): On strain assumption in a finite element model for plates and shells. Int. J. Num. Meth. Eng. 31: 287–305